

# Top-Level Design and Preliminary Physical Analysis for the First Electron-Beam Micro-CT Scanner

\*Ge Wang<sup>a,b,c,d</sup>, Yinong Liu<sup>d</sup>, Yangbo Ye<sup>a,c</sup>, Shiyong Zhao<sup>a</sup>, Jiang Hsieh<sup>e</sup>, Shuping Ge<sup>f</sup>

<sup>a</sup>CT/Micro-CT Laboratory, Department of Radiology, <sup>b</sup>Department of Biochemical Engineering,

<sup>c</sup>Department of Mathematics, University of Iowa, Iowa City, Iowa 52242, USA

<sup>d</sup>Department of Engineering Physics, Tsinghua University, Beijing, China

<sup>e</sup>Applied Science Laboratory, GE Healthcare, Milwaukee, Wisconsin 53201, USA

<sup>f</sup>The Lillie Frank Abercrombie Section of Cardiology Department of Pediatrics, Baylor College of Medicine and Texas Children's Hospital, Houston, TX 77030

**Abstract:** A state of the art X-ray micro-CT scanner takes about 20 seconds to acquire a full dataset, which is too slow to capture the rapidly beating heart of small animals. We have been working to develop the first electron-beam micro-CT (EBMCT) prototype for cardiac imaging of the mice and rats. In this paper, we describe the background on electron-beam CT (EBCT) and emphasize the needs for EBMCT. Then, we present a top-level design and a preliminary physical analysis for the first EBMCT scanner. The proposed EBMCT prototype would allow 0.03-0.01s temporal resolution (35-70 half-scans per second) with 0.2mm spatial resolution and 5% contrast resolution. Finally, we discuss a few related issues to further highlight that this project is not only important for basic biomedical research but also feasible technically.

**Key Words:** Electron-beam micro-CT (EBMCT), cone-beam, circular and spiral scanning loci, small animal imaging, cardiac imaging.

\*Corresponding author: Ge Wang

## I. Introduction

In the United States, cardiovascular diseases are the leading cause of mortality and morbidity. Traditional predictive factors for heart diseases include high cholesterol levels, high blood pressure, obesity, diabetes, and so on. It has been found that the electron-beam CT (EBCT) technology, developed in the early 1980s for cardiac imaging, significantly improves assessment of the potential risk for cardiac diseases. Because of its ultra high temporal resolution, EBCT can quantify calcification in the arteries, which is an indication of atherosclerosis. An EBCT-based coronary calcium score is of significant predictive value of heart attacks or need for bypass or angioplasty over next year or two. In addition, EBCT is also useful in evaluating bypass graft potency, congenital and acquired heart diseases, and quantifying ventricular muscle mass, chamber volumes, and systolic and diastolic functions. EBCT is now accepted as the gold standard for detecting early heart diseases and the centerpiece of the preventive cardiology program. In addition to its remarkable applications for dynamic anatomical imaging of cardiac structures, EBCT is also a powerful tool for physiological imaging.

An EBCT scanner can take cross-sectional images so quickly that the beating heart can be virtually frozen. In an EBCT scanner, a sufficient amount of fan-beam projection data is acquired within 50-100 ms, which is extremely difficult to achieve using a mechanically rotated X-ray source as commonly encountered in the third and fourth generation CT scanners. By its unique physical design, the EBCT scanner dynamically steers an X-ray source spot by sweeping an electron-beam on a tungsten arc with multiple tracks, based on the same principles of a cathode ray tube in which the electron-beam is controlled by dedicated coils. Despite its undisputable advantages, in our opinion the current EBCT techniques are subject to at least two major weaknesses. First, it is not in cone-

beam geometry and does not support standard and nonstandard spiral scanning. Second, the X-ray spot is not intensive sufficiently to produce the image quality characteristic with the mechanical rotation based scanners.

To understand etiology and pathogenesis of cardiovascular diseases as well as to develop effective prevention and treatment strategies, small animals have become some of the most common models of human diseases (Hoit 2001). For example, transgenic mice are increasingly used to probe genetic aspects of cardiovascular pathophysiology. By use of gene targeting and/or transgenesis, it is now possible to make defined changes in genes whose functions underlie mammalian cardiovascular functions. Genetic modification of the loci responsible for cardiac development and functions has begun to provide mouse models of cardiac hypertrophy, dilated cardiomyopathy, and hypertrophic cardiomyopathy. The genes that are possibly related to coronary artery diseases are also being explored.

Just as we need various tomographic imaging systems for patient studies, we also need micro-tomographic devices for small animal studies. Although there has been an explosive growth in the development of micro-CT scanners, much of efforts have been dedicated to improve spatial resolution instead of temporal resolution. Since the 1990s a large number of micro-CT systems have been constructed. Most of them employ CCD cameras and micro-focus x-ray tubes to produce image resolution from a few  $\mu\text{m}$  to hundreds  $\mu\text{m}$ . In modern micro-CT systems, the data acquisition system rotates about an animal table, while in earlier systems an animal stage is rotated in a fixed data acquisition system. These imaging systems permit screening of small animals for mutations or pathologies, and monitoring disease progression and response to therapy. *However, currently an X-ray micro-CT scanner takes at least 20 seconds to acquire a full dataset. To date there is little effort for development of an ultra fast micro-CT scanner to study dynamic processes in small animals.*

To address this grand challenge for small animal imaging, last year Wang and Ye proposed to develop the first electron-beam micro-CT (EBMCT), and filed a patent disclosure with the University of Iowa Research Foundation, entitled “*Nontrivial Spiral Cone-Beam Scanning Methods, Apparatus, and Applications*” (Wang and Ye 2003). This year they filed a provisional patent application based on that disclosure (Wang and Ye 2003). The primary goal of this paper is to demonstrate the technical feasibility of the proposed EBMCT scanner. In the following section, we report a top-level design of the proposed scanner. In the third section, we present a physical analysis to support the selection of the system parameters, with an emphasis on the source and the detector. Finally, we discuss a number of related issues, and conclude the paper.

## II. Top-Level Design

**[Electron-beam source]** There are several implementation problems related with electron-beam techniques (Boyd and Lipton 1983, McCollough 1995, Hsieh 2003). The space charge of the electron-beam becomes neutralized by the beam-generated plasma in less than a scan time. Thus, the stability of electron-beam focusing is essential. Nitrogen gas may be filled into the chamber so that the neutralization saturates before the beam reaches the active part of the target. Ion clearing electrodes ensure that the beam can be selectively self-focusing or self-defocusing. Aberration-free focusing requires that the beam phase space satisfy a certain condition. Residual aberrations due to non-uniformities are corrected by manipulating the boundary between the neutralized and space charge dominated sections of the beam.

Similar to EBCT, in EBMCT bremsstrahlung X-rays are produced by de-accelerating electrons in a tungsten-based target (alloy containing tungsten and other appropriate metallic components). Such an X-ray spot can also be steered continuously or in a stepping fashion. The scanning locus is defined by the geometric arrangement of a curvilinear metallic target. The voltage difference between the electron gun (ground) and the target (positive potential) will be adjusted to be significantly softer (30-80kV) than that of conventional CT scanner (120-250kV). The initial energies of X-rays can be

calculated from the published X-ray spectra of various target/filter materials. A nonstandard spiral scanning is preferred for the EBMCT system, including not only spiral-like loci but also circular loci, standard and nonstandard saddle curves. The electro-magnetic deflection system will be designed to control the focal spot up to a high accuracy.

With the X-ray spectrum for micro-CT of small animals, about 99% of the energy becomes heat on the spot, propagating into adjacent areas and the vacuum housing of the system. A direct contact water cooling system will be used to remove heat quickly from the base material so that multiple spiral cone-beam scans can be repeated without any overheating problem.

**[Area detectors]** There are a large variety of area detectors, including thin-film transistors (TFT,  $\alpha$ -Si:H) and mono-crystalline silicon CCD/CMOS detectors. Although the quantum efficiency of TFT detectors is high, its readout speed is generally less than 30 frames per second, rarely reaching 100 frames per second. On the other hand, the readout speed of CCD/CMOS detectors can be extremely high such as 10,000 frames per second, but they must be coupled with fiber-optical tapers with a low quantum efficiency. A good choice is the 1000 Series camera from Spectral Instruments (<http://www.specinst.com/>), which can be not only directly used but also adapted to meet our special requirements. The size of this camera is 92 by 92 by 168 mm. Two, three, and four-phase architecture CCDs can be placed in the camera. The readout and digitization uses a 16-bit digitizer. The pixel readout rate can be 50kHz to 1MHz. The gain of the analog processor can be modified under computer control to compensate for the gain change of the dual slope integrator at different readout speeds. This camera offers fully programmable readout of sub-arrays and independent register binning. In addition, specialized readout modes, such as time delay and integration using an internal or external time base are possible. These capabilities allow the readout of only the area of the CCD of interest at variable resolution.

The detector noise ratio is a key factor to assess the data acquisition system (DAS). There are three types of noise: photon noise, dark noise, and read noise. *Photon noise* is realized by detectors that convert incoming photons into photoelectrons. The number of photoelectrons obeys a Poisson distribution and relates to SNR by a square root relationship. *Dark noise* is temperature dependent, due to thermally generated electrons within the detector architecture. The number of thermal electrons also obeys a Poisson distribution. *Read noise* happens in the DAS circuitry. The on-chip preamplifier produces a primary part of read noise. Spurious charge also makes a significant contribution. When the number of photons is sufficiently small, read noise would exceed photon noise, which is referred to as "read-noise limited". Similarly, we can define the most common case "photon-noise limited". In this project, we assume that the detector noise is about 1,000 electrons.

**[Reconstruction methods]** Both exact and approximate algorithms have their relative merits in terms of image quality, and have been extensively studied over past two decades. In 1984, Feldkamp *et al.* proposed an approximate cone-beam algorithm for circular cone-beam scanning. In 1991, Wang *et al.* generalized the Feldkamp algorithm for cone-beam scanning along various scanning loci, which works well for spherical, rod-like or plate-shaped objects with various scanning loci including nonstandard spirals (Wang *et al.* 1991, 1993). Recently, Katsevich derived the first theoretically exact reconstruction formula for the helical cone-beam geometry in the filtered backprojection format. Then, we studied cone-beam CT projections along a nonstandard 3D spiral with variable radius and variable pitch. Specifically, we generalized both the filtered backprojection method and the backprojected filtration method from the standard helical scanning case to the nonstandard spiral scanning cases (Katsevich 2004, Ye and Wang 2003, Ye *et al.* 2004, Zou and Pan 2004). Our proofs are independent of the shape of the spiral, as long as the object is contained in a region inside the spiral, where there is a generalized PI line passing through any interior point (that is, a smooth scanning curve goes from one end point to the other end point of the generalized PI line). We performed numerical simulation and demonstrated the correctness of these generalized exact cone-beam reconstruction formulas (Yu *et al.* 2004). Furthermore, we may use statistical methods for image reconstruction, which are typically iterative (Jiang and Wang 2002, Li *et al.* 2003).

**[System configuration]** The system architecture is illustrated in Figure 1. The side view emphasizes the geometry between the electron gun and the tungsten target locus. Magnetic coils must precisely focus and steer the electron beam through the evacuated drift tube. The cross-sectional view is seen from the perspective of the incoming electron beam. The electron beam strikes the tungsten target at an upper left location, and are spirally scanned over multiple spiral turns. In addition to the spiral curvilinear target, other configurations are also feasible, such as circular loci, standard and nonstandard saddle curves. The pre-target collimation may be necessary but has not been shown for brevity. The area detector supported enclosure acquires the cone-beam data during the nonstandard spiral scan. The optical tapers are needed for coupling the CCD cameras for a maximum coverage. The cameras are configured outside the vacuum chamber, and cooled to reduce the detector noise. Note that this design can be modified to allow other non-standard spiral loci, such as saddle curves (Pack *et al.* 2003)

### III. Physical Analysis

**[Temporal resolution]** Briefly speaking, in terms of temporal resolution our EBMCT prototype will improve the EBCT by several folds to an order of magnitude, outperform the current micro-CT by several orders of magnitudes. The cardiac rates of mice and rats are much higher than that of the human (Yang 1999, Watson 2004), as summarized in Table 1. As a representative case, let us assume a cardiac rate of 7 beats per second, which is about 5 times higher than that of the human. Then, we require 5-10 CT images per cardiac cycle, which means 0.03-0.014s temporal resolution or 35-70 CT images per second. Given the limited power of the X-ray source, the constrained readout speed of the detector and the radiation exposure consideration, we will strive for the high temporal resolution while somehow relaxing the requirements for spatial and contrast resolution. If the diameter of the cardiac region of a mouse is 10mm, we can cover the area of 10 by 10 mm with 100 by 100 detector cells (100 $\mu$ m detector size). To produce a satisfactory local reconstruction of an image volume of 100 by 100 by 100 voxels, 100 cone-beam projections should be sufficiently high. Actually, according to the recent results on MRI VIPR (a magnetic resonance imaging technique using *Vastly undersampled Isotropic PROjection*) (Barger *et al.* 2002), 60 cone-beam projections should be workable for adequate image quality. Assume that the diameter of the mouse thorax is 30mm, each cone-beam view would roughly consist of 300 by 300 detector cells. Therefore, the number of cone-beam projections of 300 by 300 elements would be 2100 (35 by 60) to 4,200 (70 by 60) per second. Because the detectors are stationary and at each instant about 1/3 of them are in use, the detector readout speed would be about 700-1,400 frame per second.

**[Contrast resolution]** The contrast resolution may be defined as the percentage of the mean difference between a region of interest and the background relative to the background (Cohen 1979, Hanson 1977, Sekihara 1982). Because the EBMCT scanner emphasizes the temporal resolution, the contrast resolution is not pushed to be most sensitive. As an initial choice, we set the contrast resolution to 5%. To distinguish a region of interest with a 50% confidence, we have the empirical

relationship  $C = k \frac{\Delta p}{D} \frac{\sigma}{\mu_b}$ , where  $C$  denotes the contrast resolution,  $k$  a constant between 2 and 5,

$\Delta p$  the pixel size,  $D$  the diameter of the target of interest,  $\sigma$  noise and  $\mu_b$  the background mean (Cohen 1979, Hanson 1977, Sekihara 1982). Here we set  $C = 5\%$ ,  $k = 3.5$ ,  $\Delta p = 0.1mm$ ,  $D = 1mm$ , and obtain the signal-to-noise ratio SNR  $\mu_b / \sigma \approx 7$ .

Because the noise distribution is quite complicated over the field of view, we use the noise at the center of a water disk in this feasibility analysis. According to the well-known Barrett formula (Barrett 1983):  $SNR = 0.665 \mu_0 \delta^2 \sqrt{M n_0 e^{-2\mu_0 R}}$ , where  $\mu_0$  denotes the linear attenuation coefficient,  $\delta$  the

spatial resolution,  $M$  the number of projection views,  $n_0$  the number of incoming photons per unit length, and  $R$  the object radius. Here we set  $\mu_0 = 0.37(\text{cm}^{-1})$  for water at 30kV,  $\delta = 0.2\text{mm}$ ,  $M = 60$ ,  $R = 25\text{mm}$ , and obtain the photon density  $n_0 \approx 2.2 \cdot 10^4$  photons  $\text{mm}^{-1}$ . Assuming cubic voxels for EBMCT, we obtain the number of incoming photons per unit area as  $n_0 / \delta \approx 1.1 \cdot 10^5$  photons  $\text{mm}^{-2}$ . Since the frame rate is about 700-1,400 frames per second, the rate of the photon area density should be about  $10^8$  photons  $\text{mm}^{-2}\text{s}^{-1}$ . According to our Monte-Carlo simulation data in Table 2, the output at the distance of 1 meter away from the focal spot of an X-ray tube operated at 30kV is about  $7 \cdot 10^5$  photons  $\text{mm}^{-2} (\text{mAs})^{-1}$ . With a 100mm source-to-detector distance, we should have  $7 \cdot 10^7$  photons  $\text{mm}^{-2} (\text{mAs})^{-1}$  near the detector plane. Therefore, the tube current should be about 2-10mAs, with some conservative considerations that photons in this energy range are more subject to absorption in the vacuum chamber wall and so on.

**[Spatial resolution]** The spatial resolution of the EBMCT system can be estimated from the focal spot blurring  $B_f$  and detector blurring  $B_d$ , which are functions of the magnification of the system and approximately given by  $B_f = f(M - 1) / M$  and  $B_d = d / M$  respectively, where  $f$  denotes the inherent focal spot size,  $d$  the size of the detector cell, and  $M$  the magnification factor of the system defined as the ratio of the source-to-detector distance and the source-to-axis distance. The spatial resolution of the system is the square root of the sum of the squares of the individual blurring components (Yester 1977). For example, with about 250 $\mu\text{m}$  focal spot, 150 $\mu\text{m}$  detector size (binning mode) and 3 fold magnification, about 180 $\mu\text{m}$  spatial resolution can be obtained.

The finite area of the X-ray focal spot causes structural details be smeared, leading to the *source blurring*. The spot size also varies with the applied tube voltage ( $U$ ) and current ( $I$ ). It was found that the size of the focus spot could be modeled as proportional to  $I$  and inversely proportional to  $U^{3/2}$ . In the current EBCT the beam spot size is between 0.6mm to 1.2mm in the azimuthal direction and between 1.1mm to 1.4mm in length for 130kV and 140kV protocols. The high voltage supply would stay within 0.1% of the nominal voltage. The spot intensity distribution can be modeled as being circular and Gaussian. Given the current technology we estimate that the focal spot size would be around 0.2-0.3mm in diameter. Actually, the focus spot may be asymmetric due to the nonstandard nature of the spiral locus and the imperfect focusing of the electron-beam. As a result, the focal spot may vary spatially.

The source blurring may be a limiting factor, but it can be compensated for with some collimated source techniques and/or digital deconvolution methods. The source collimation can be achieved if we can design an effective target configuration for the X-ray spot not to be spread widely. This may be implemented by a sophisticated fabrication of the target in which the tungsten-based material is only limited to the desirable positions along the nonstandard spiral structure of much less efficient X-ray generating material. When a relatively large focus spot size is used for our proposed EBMCT system, we can develop source-deblurring algorithms to reduce the source size retrospectively. When the size of a field of view is small relative to its distance from the X-ray source, the weak perspective model is quite accurate. Under the weak perspective, a divergent beam projection can be well approximated as a scaled parallel-beam projection. Consequently, the spatially variant blurring model due to the finite size of the X-ray source can be simplified as a spatially invariant blurring model. We will first invert such a simplified source-blurring model. If it becomes necessary, fully 3D iterative deblurring methods can be developed assuming a spatially variant imaging model.

**[System parameters]** Some key parameters of the prototype system are listed in Table 3. Note that we give the ranges of these parameters to allow not only some engineering flexibilities but also various small animal imaging modes. After a dataset is acquired, the image quality indexes are not uniquely defined. To a substantial extent, these indexes can be traded off and optimized by using

appropriate reconstruction and post-processing algorithms. We may tailor these indexes to best suit specific requirements. Also, in addition to cone-beam reconstruction our proposed system can also be used in other modes, such as cone-beam tomosynthesis and digital subtraction angiography.

#### IV. Discussions and Conclusion

As an alternative way to demonstrate the feasibility of the proposed EBMCT prototype, we can analyze the needed SNR of the EBMCT by extrapolating the EBCT data. Let us assume that the tube voltages are 30kV for EBMCT and 120kV for EBCT, respectively. The modified Fewell spectra are plotted in Figure 2, which gives the distributions of the X-ray photon number per energy bin. According to Figure 2, the number of X-ray photons generated by 30kV and that by 120kV can be roughly estimated as 70,000 and 3,000,000, respectively. Then, let us assume that the mouse and the human are roughly modeled as water phantoms of diameters 3cm and 30cm, respectively. The linear attenuation coefficients of water at 30kV and 120kV are 0.161/cm and 0.376/cm, respectively. For clarity, we have the key parameters summarized in Table 4. Hence, the ratio between the 30kV and 120kV numbers of incoming photons is about 1/43. On the other hand, the ratio between the total attenuation rates of the mouse and human phantoms is about 40.5. Therefore, with the EBCT imaging parameters the SNR of the EBMCT should be about the same as that of the EBCT. Then, we can improve the X-ray photon statistics up to two orders of magnitude by reducing the size of the EBCT scanner down to about 1/10 of its dimensions. Given this leverage we can increase the scanning time by about 10 times and decrease the detector area by 10 times for EBMCT to have a comparable signal-to-noise ratio as that of EBCT.

As seen in Table 1, the heart rates in anesthetized mice are approximately 45% of those of conscious mice (Yang 1999). Further pharmacological maneuvers such as  $\beta$  blockade of the sympathetic pathways may further reduce heart rates if needed. In this project, we propose to scan rats and mice under general anesthesia with further  $\beta$  blockade as needed for dynamic volumetric imaging using EBMCT. We can also increase the voltage for an improved SNR. The higher the voltage, the less the attenuation coefficient but perhaps poorer the contrast resolution. Another way to improve the imaging performance of EBMCT is to employ two or three electron guns positioned on the same side but largely separated and magnetically masked, each of which independently scans appropriate segments of the common tungsten-based target. This will effectively refine the temporal resolution triply. Moreover, we may use a flat electron-beam to hit the target at multiple locations simultaneously to reduce the scanning time further.

While it can be regarded as a miniature of the well-known EBCT scanner, the EBMCT system is based on several proprietary technologies of our CT/Micro-CT Laboratory (Wang and Ye 2003). Technically, its electron-beam traces a nonstandard spiral locus at an unprecedented speed, and produces cone-beam projections for dynamic and volumetric image reconstruction. Clinically, its functionalities directly meet one of the major challenges in the area of small animal imaging, which can be instrumental for cardiac studies. Although this project is exploratory, we believe that the efforts along this direction are well justified and the results promising.

It is highly likely that ultra-fast CT may become the modality of choice for cardiac imaging of small animals. Currently, cardiac ultrasound has been the method of the first choice for human and large animals. In principle, cardiac ultrasound is useful to derive qualitative and quantitative data for the cardiac anatomy and function. Cardiovascular flow information can also be obtained using Doppler echocardiography. However, the cardiac ultrasound method is seriously limited by its acoustic windows and image quality, which is often blurry, noisy and subject to artifacts. The high carrier frequency ultrasound device may improve the near field resolution but the penetration is limited, and the image quality in the far field as well as the Doppler capabilities are often significantly compromised. Current cardiac ultrasound devices for small animal imaging are 2D only, which limit quantitative accuracy for assessment of alterations in cardiac functions due to genetic or

pharmacological interventions. Although magnetic resonant imaging (CMRI) is a valuable tool for small animal imaging, the image acquisition is significantly slower than ultra-fast X-ray CT. For example, it takes about 2 minutes to acquire the images to achieve a 0.2 by 0.4 mm 2D resolution with a slice thickness of 2 mm using a 4.7T MRI scanner (Nahrendorf *et al.* 2003).

In conclusion, we have proposed the first EBMCT prototype for cardiac imaging of the mice and rats, presented a top-level design and a preliminary physical analysis, and demonstrated that such a scanner is technically feasible. Currently, we plan to select small animal models of cardiac diseases, evaluate the effect of anesthesia and possibly beta blockade on the cardiac rates, collect real data using the EBCT scanner, and optimize the design of the EBMCT prototype. We believe that the EBMCT should be the method of choice to meet the ultra-fast imaging needs in the area of small animal cardiac studies.

### **Acknowledgment**

This work was partially supported by NIH/NIBIB grants (EB002667 and EB004287) and a Carver Scientific Research Initiative grant from University of Iowa.

## References

- Barger AV, Block WF, Toropov T, Grist TM, Mistretta CA: Time-resolved contrast-enhanced imaging with isotropic resolution and broad coverage using an undersampled 3D projection trajectory. *Magn. Reson. Med.* 48:297-305, 2002
- Barrett HH, Swindell W: *Radiological Imaging, Vol 2*, Academic Press, New York, NY, 1981
- Boyd DP, Lipton MJ: Cardiac computed tomography. *Proc. IEEE* 71:298-307, 1983
- Cohen G, DiBianca F: The use of contrast-detail-dose evaluation of image quality in a CT scanner. *Journal of Computer Assisted Tomography* 3:189–195, 1979
- Hanson KM: Detectability in the presence of computed tomographic reconstruction noise. *Proc. SPIE Vol 27*, 304–312, 1977
- Hoit BD: New approaches to phenotypic analysis in adult mice. *J Mol Cell Cardiol.* ;33:27-35, 2001
- Hsieh J: *Computed Tomography Principles, Design, Artifacts, and Recent Advances*. SPIE Press, 2003
- Jiang M, Wang G: Development of iterative algorithms for image reconstruction. *Journal of X-Ray Science and Technology* 10:77-86, 2002
- Katsevich A: An improved exact filtered backprojection algorithm for spiral computed tomography. *Adv. Appl. Math.* 32:681-697, 2004
- Li X, Jiang M, Wang G: A numerical simulator in VC++ on PC for iterative image reconstruction. *Journal of X-Ray Science and Technology* 11:61-70, 2003
- McCullough CH: Principles and performance of electron beam CT. *Medical CT and Ultrasound: Current Technology and Applications*, ed. LW Goldman and JB Fowlkes, Advanced Medical Publishing, 487-518, 1995
- Nahrendorf M, Hiller KH, Hu K, Ertl G, Haase A, Bauer WR: Cardiac magnetic resonance imaging in small animal models of human heart failure. *Med. Image Anal.* 7:369-375, 2003
- Pack JD, Noo F, Kudo H: Investigation of a saddle trajectory for cardiac CT imaging in cone beam geometry. *Proc. 2003 Meeting on Fully 3D Image Reconstruction in Radiology and Nuclear Medicine*, 2003
- Sekihara K., Kohno H, Yamamoto S: Theoretical prediction of X-ray CT image quality using contrast detail diagrams. *IEEE Transactions on Nuclear Science* 29:2115–2121, 1982
- Wang, G, Lin, TH, Cheng PC, Shinozaki DM, Kim, HG: Scanning cone-beam reconstruction algorithms for x-ray microtomography. *Proc. SPIE Vol. 1556*, 99-112, July 1991
- Wang G, Lin TH, Cheng PC, Shinozaki DM: A general cone-beam reconstruction algorithm. *IEEE Trans. on Medical Imaging* 12:486-496, 1993
- Wang G, Ye Y: Nonstandard spiral cone-beam scanning methods, apparatus, and applications, Patent disclosure filed with University of Iowa, November 2003 (US Provisional patent application pending)
- Watson LE, Sheth M, Denyer RF, Dostal DE: Baseline echocardiographic values for adult male rats. *J Am Soc Echocardiogr.* 17:161-7, 2004
- Yang XP, Liu YH, Rhaleb NE, Kurihara N, Kim HE, Carretero OA: Echocardiographic assessment of cardiac function in conscious and anesthetized mice. *Am J Physiol.* 277(5 Pt 2):H1967-74, 1999
- Ye Y, Zhao S, Yu H, Wang G: Exact image reconstruction for cone-beam CT along nonstandard spirals and other curves. *Proc. SPIE Vol. 3353*, August 2004, in press
- Yester, MW, Barnes GT: Geometrical limitations of computed tomography (CT) scanner resolution. *Proc. SPIE Vol 127*, 296–303, 1977
- Yu H, Ye Y, Wang G: Katsevich-type algorithms for variable radius spiral cone-beam CT. *Proc. SPIE Vol. 3353*, August 2004, in press
- Zou Y, Pan X: Exact image reconstruction on PI lines from minimum data in helical cone-beam CT. *Phys. Med. Biol.* 49, 941-959, 2004

Table 1. Cardiac rates, heart and body diameters of the mouse and the rat (LVEDD: Left ventricular end diastolic diameter) (Yang 1999, Watson 2004).

|              | Heart Rate (bpm)                               | LVEDD (mm)  | Body Diameter (mm) |
|--------------|--|---|--------------------|
| <b>Rat</b>   | 292.9 ± 36.0                                   | 5.5 ± 0.8   | ~50                |
| <b>Mouse</b> | 658 ± 9 (conscious)<br>293 ± 19 (anesthetized) | 2.52 ± 0.06 (conscious)<br>3.57 ± 0.09 (anesthetized) | ~30                |

Table 2. Measured and simulated X-ray photon flux data in air upon 1mm<sup>2</sup> detector area.

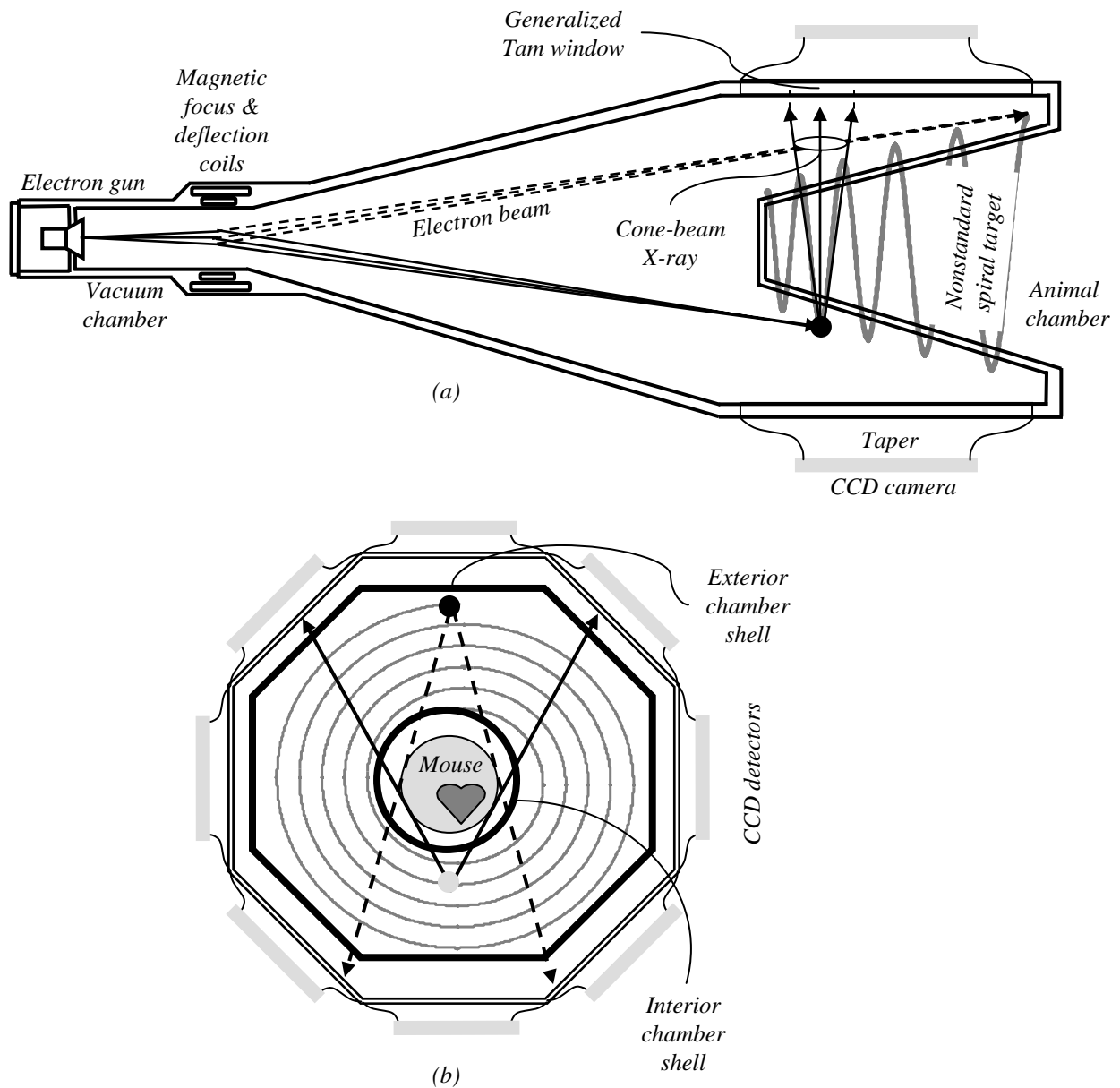
| Tube voltage (kV)  | Distance (mm)                           | Flux (s <sup>-1</sup> )  | Average energy (keV) |
|--|---|--------------------------|----------------------|
| <b>Monte-Carlo simulation with an EBCT Simulator of GEHC (100mA)</b> |   |                          |                      |
| 90   | 1,575                                   | 2.53976x10 <sup>10</sup> | 50.6                 |
| 140  | 1,575                                   | 1.08447x10 <sup>11</sup> | 63.6                 |
| <b>Monte-Carlo simulation with a CT Simulator of GEHC (100mA)</b>    |   |                          |                      |
| 30   | 949                                     | 7.45145x10 <sup>7</sup>  | 13.6                 |
| <b>Physical measurement on a GE CT scanner (100mA)</b>               |   |                          |                      |
| 120  | 949                                     | 5.23060x10 <sup>8</sup>  | 67.0                 |
| <b>Dose (mR/mm<sup>2</sup>)</b>                                      | 2.15 (891mm from source without bowtie) |                          |                      |

Table 3. Parametric ranges for the EBMCT prototype.

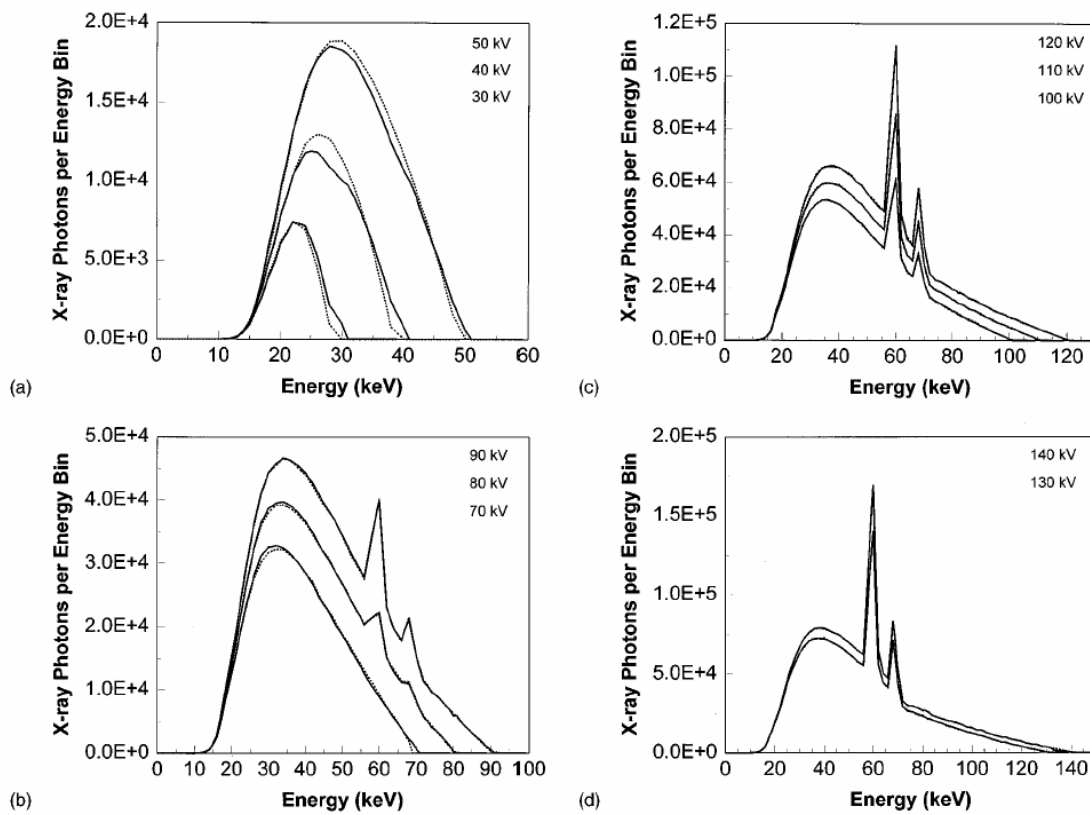
|  |                            |                        |                  |                       |                          |
|--|----------------------------|------------------------|------------------|-----------------------|--------------------------|
| <b>Source to Axis Distance, M</b>        | 40-60mm, 2-3               | <b>Target Material</b> | Tungsten - based | <b>Camera Head</b>    | Spectral Instrument 1000 |
| <b>Number of Views per Half-Scan</b>     | 60-100                     | <b>Tube Voltage</b>    | 30-80kV          | <b>Detector Cell</b>  | 50-200 μ m               |
| <b>Spatial &amp; Contrast Resolution</b> | 200 μ m, ~5%               | <b>Tube Current</b>    | 2-10mA           | <b>Frame Speed</b>    | 700-1,400fps             |
| <b>Scanning Speed</b>                    | 25-50Hz (35-70 half-scans) | <b>Focus Spot</b>      | 50-200 μ m       | <b>Detector Noise</b> | ~1000 electrons          |

Table 4. Key parameters for analyzing signal-to-noise ratios of EBMCT and EBCT.

| Voltage (kV) | Photon Number | Attenuation (cm <sup>-1</sup> ) | Diameter (cm) |
|--------------|---------------|---------------------------------|---------------|
| 30           | 70,000        | 0.376                           | 3             |
| 120          | 3,000,000     | 0.161                           | 30            |



**Figure 1.** Conceptual diagram of the proposed electron-beam micro-CT (EBMCT) prototype. (a) Longitudinal cross-section of the prototype. The magnetic coils focus and deflect the electron-beam through the evacuated chamber along a nonstandard spiral tungsten-based curvilinear structure to produce cone-beam projection in a generalized Tam window. (b) Transverse cross-section of the prototype. Eight CCD detector plates enclose the nonstandard spiral target to receive cone-beam data at an extremely high speed. Note the drawings are not made to scale for clarity.



**Figure 2.** The modified Fewell spectra are plotted (dashed lines) and compared with the corresponding TASMIP-generated spectra (solid lines). The TASMIP algorithm produces spectra that are accurate in terms of both spectral shape (quality) and spectral amplitude (quantity). Both properties are compared in this figure (adopted from Boone JM, Seibert JA: An accurate method for computer-generating tungsten anode x-ray spectra from 20 to 140 kV. *Med. Phys.* 24:1661-1670, 1997).